# Meniscus Control by String in Roll Coating Experiment

**M. Decré, E. Gailly, and J.-M. Buchlin**
von Karman Institute for Fluid Dynamics, Ch. de Waterloo, 72, B 1640 Rhode-Saint-Genèse, Belgium

*The ribbing instability hinders the roll coating process, as it produces wavy coating films. The technique studied here prevents ribbing, whereby a string is placed parallel to the rolls, in contact with the unstable meniscus. In this experiment, the fluid is a Newtonian oil. A free-surface visualization technique allows measurement of the interface profile where the string interacts with the forming films. The ribbing can be eliminated under conditions at least 20 times its natural onset. The influence of the string position on the mass transfer is then examined. Measurements show that the streamwise position of the string controls the total flow rate of the process, while its transverse position accurately controls the relative thicknesses applied on each roll. The string proves to be both an efficient concept to eliminate ribbing, and a reliable way of fixing the coating film thickness, without resorting to traditional gap width and roller speeds selection.*

## Introduction

In asymmetric roll coating experiments, a liquid is entrained in the narrow gap separating two horizontal, rotating cylinders. The roller radii are different, as are usually their tangential velocities. Downstream of the gap of width $h_o$, the flow separates into two films coating each cylinder; these films are connected by a meniscus (Figure 1). The technology of coating is widely used in the photographic and magnetic tapes industries, as well as metallic strip coating in the metallurgic industry. In the latter applications, the substrate is entrained by one cylinder and consequently coated at the outlet of the gap. Industrialists wish both to control the amount of liquid applied on the substrate and to obtain a uniform coating layer.

Several studies (Savage, 1982; Coyle et al., 1986; Adachi et al., 1988; Decré et al., 1995a) have shown that the film thicknesses are functions of the tangential velocities of the rolls $U_i$ and of the gap width. These variables are present in three controlling dimensionless groups, namely the gap ratio $G = h_o/R$, where $R = 2\,R_1R_2/(R_1 + R_2)$ is the radius of an equivalent setup with symmetric rolls, and two capillary numbers $Ca_i = \mu U_i/\sigma$ for independently rotating cylinders. The isothermal, Newtonian fluid is characterized by its dynamic viscosity $\mu$, its surface tension $\sigma$, and its specific mass $\rho$. The mean capillary number $Ca_m = (Ca_1 + Ca_2)/2$ and the speed ratio $S = Ca_1/Ca_2$ are also occasionally used instead of the pair $(Ca_1, Ca_2)$. The subscripts 1 and 2 refer to the upper and lower cylinders, respectively.

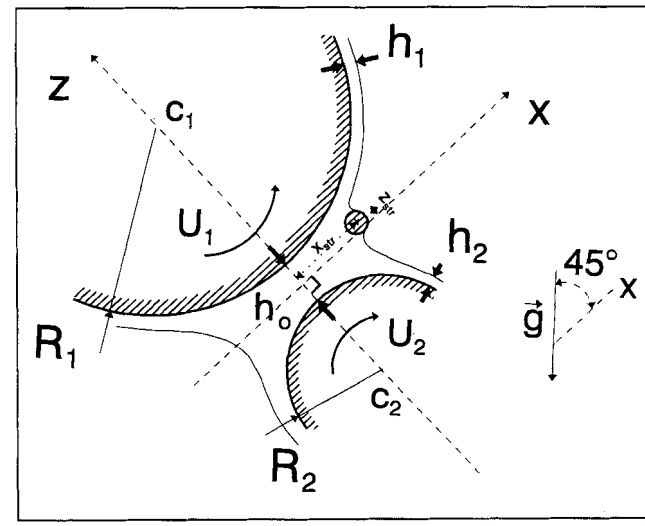


**Figure 1. Cross section of the roll coating rig.**

When $G$ and $S$ are kept constant, a stationary, periodic instability called ribbing perturbs the meniscus when the capillary numbers exceed critical values $(Ca_1^{crit}, Ca_2^{crit})$ (Benkreira et al., 1982; Savage, 1984; Carter and Savage, 1987; Coyle et al., 1990; Rabaud et al., 1990). Further above its

onset threshold, the ribbing undergoes secondary instabilities leading to complex spatio-temporal behaviors and eventually chaos (Michalland et al., 1993; Decré et al., 1995b). A recent study of asymmetric coating from basic flow properties to chaotic behaviors has been made by Decré (1994).

The aforementioned works have shown that, under operating conditions compatible with production requirements of the present day, roll speeds are such that ribbing is always present. As a consequence, coating engineers have concentrated their efforts on removing ribbing particularly by improving leveling of the coating before it dries. Many solutions lead to the use of additives, which can amount up to 0.5 volumetric fraction of the coating liquid. The present work investigates a concept that prevents ribbing from appearing whatsoever. Hasegawa and Sorimachi (1993) have recently proposed to place a string along the cylinders so as to touch the unstable meniscus. However, their demonstration of the elimination of ribbing was made with a hand-stretched nylon fishing line, so that no quantitative conclusions could be drawn.

The present study is at the development stage of the string concept. It aims at quantitatively understanding the correlation between the position of the string ($x_{str}$, $z_{str}$) (see the orthonormal coordinate system defined in Figure 1) and the basic coating mechanisms, i.e., ribbing, total flow rate, partial flow rates on individual cylinders, and contact line properties. To this end, a free-surface visualization technique—already successful in measuring natural, stable coating menisci (Decré et al., 1995a)—is applied to obtain experimental cross-sections of menisci controlled by a string. This is performed for several capillary number combinations otherwise displaying ribbing. These measurements, along with accurate film thickness measurements and film profile measurements using a standard commercial device, provide clear, quantitative evidence of the efficiency of the string to eliminate ribbing. The effect of the position of the string relative to the cylinders on the mass transfer is then documented. From these measurements, it is concluded that the streamwise position of the string controls the total flow rate, while its transverse position controls the relative flow rate on each cylinder. Evaluation of wetting conditions at the contact line between film and string are also performed, but interpretation of the results should be made with greatest care.

## Experimental Apparatus and Procedure

The experimental apparatus has already been described in detail in previous studies of the free meniscus without string (Decré and Buchlin, 1994; Decré et al., 1995a). It consists of two stainless steel cylinders, 260-mm long, with radii $R_1 = 67.5$ mm and $R_2 = 27.5$, mm, respectively (see Figure 1). Each cylinder is driven by an independent direct current motor, providing tangential speeds from 7 to 500 mm/s.

Each side of the frame is fitted with a pair of transversing mechanisms, wearing arms to accurately control the position of the string with respect to the cylinders. The string is positioned with a precision of 0.01 mm along $x$ and $z$, yielding a parallelism better than 0.01%. The string is a nylon P077, $\phi = 0.92$-mm dia. (Rhône-Poulenc) coated with an LW 432 H (Henkel) ethoxyled product. The tension of the string is not controlled.

The fluid under study is a Rhodorsil 47V500 silicone oil (Rhône-Poulenc), with $\mu = 0.57$ Pa·s, $\sigma = 0.021$ N/m, and $\rho = 970$ kg/m$^3$. Some methine dye (Yellow Oracete 8GF (Ciba-Geigy)) is diluted in the oil to provide Argon ion laser fluorescence.

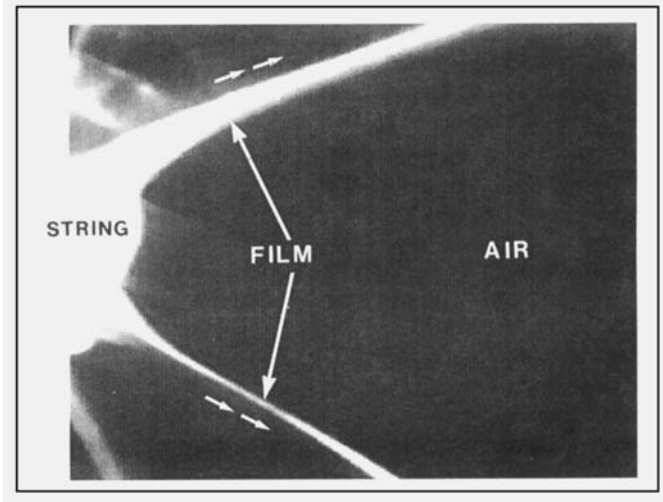


**Figure 2. Meniscus controlled by a string.**

Experimental conditions and configuration are given in caption of Figure 5.

Two measurement techniques are used in this study. First, the thickness profile along the top generatrix of the upper cylinder is measured by means of the commercial thickness measurement device ODS (Decré et al., 1995a). This allows measurement of a ribbed profile (or the absence of ribs) with an accuracy of $\pm 6.7$ $\mu$m. The second technique uses a thin Ar laser sheet ($0{,}1 \times 25$ mm$^2$) at the locus of interest to visualize a thin slice of fluorescent liquid, equidistant from both cylinder edges. It is then possible by means of a microscope to record video images of the interface which are subsequently processed (Figure 2). The absolute accuracy on the experimental meniscus profiles is 30 $\mu$m. This technique has already been successfully used in the case of free menisci, and is described in detail elsewhere (Decré and Buchlin, 1994; Decré et al., 1995a).

## Results

### *Elimination of ribbing*

The first step of this study is to investigate how efficient the string is in eliminating ribbing. The scenario of removal of the ribbing is illustrated in the sequence of photographs of Figure 3, showing a closeup along the gap separating the rolls. The working parameters are $Ca_1 = 1.0$, $Ca_2 = 3.0$, $G = 0.0163$, approximately three times above threshold (Decré, 1994). On the top picture, the string (the bright, horizontal line indicated by an arrow) has just come into contact with the lower part of the ribbed profile. It is then driven, from top to bottom, 1 mm toward the gap until ribbing is fully removed. Ribbing elimination is achieved approximately when the string reaches the trough of the ribbing waves. A striking feature of this scenario is the building up of small air cavities beneath the string, which then close to form bubbles (third image from top). These bubbles are eventually ejected when the string is pushed further towards the gap.

In order to obtain quantitative demonstration of the technique, differential thickness distribution profiles are mea-

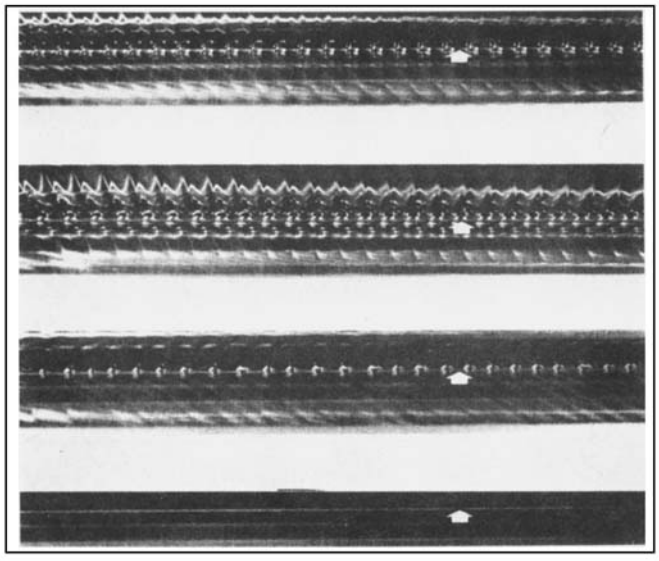

**Figure 3. Removal of ribbing when the string is pushed progressively toward the gap.**

Total ribbing amplitude 1 mm; the string is indicated by a white arrow. $Ca_1 = 1.0$, $Ca_2 = 3.0$, $G = 0.0163$.

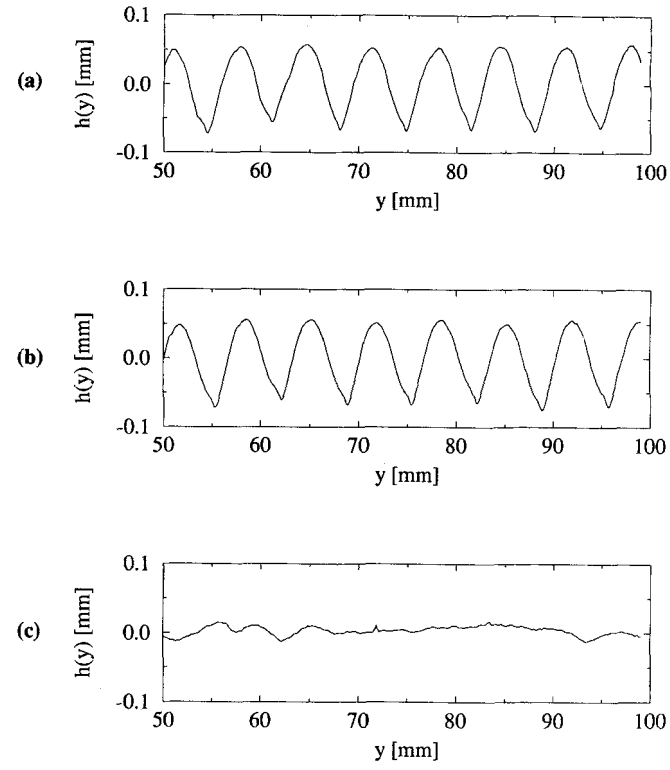


**Figure 4. ODS measurement of the differential thickness $h = h_1(y) - \overline{h_1}$ profile for several positions of the string.**

(a) String in contact with ribbing crests, average film thickness $\overline{h_1} = 0.206$ mm, ribbing amplitude $A \approx 0.1$ mm; (b) string 1.5-mm deeper, $\overline{h_1} = 0.206$ mm, $A \approx 0.1$ mm; (c) string 3.0-mm deeper, $\overline{h_1} = 0.206$ mm, $A$ negligible. $Ca_1 = 1.24$, $Ca_2 = 1.46$, $G = 0.0041$.

sured with the ODS probe along a generatrix of the rolls located sufficiently close to the string to minimize leveling. This is done for successive positions of the string (Figure 4). Under these operating conditions, the ribbing has amplitude $A = 3 \pm 0.1$ mm and wavelength $\lambda = 7 \pm 0.1$ mm. On this figure, $y$ is the coordinate along the axis of the cylinders; $h = h_1(y) - \overline{h_1}$ is the differential thickness. It is clearly seen in Figure 4c that, to the accuracy of the probe, ribbing has been fully removed. It has been possible to remove ribbing in this manner up to working conditions at least 20 times above threshold, without any sign that it should not be possible at even higher values.

As will be discussed at length in the following sections, the stabilized interface consists of two independent films attached to the string at an apparent contact line as shown in Figure 5. As the string goes deeper into the gap, the contact lines get closer to each other (see the section discussing apparent contact lines). The contact lines eventually meet and recreate a free, ribbed meniscus, while the string is fully immersed. Contact hysteresis is also observed: if $x_{stab}$ is the first streamwise string position at which ribbing disappears, it is possible once this condition is fulfilled to move the string away from the gap at $x_{str} > x_{stab}$ without destroying the stability until the meniscus ultimately detaches from the string.

### *Effect of string position*

As discussed in the previous section, there exists a range of string positions within which the string, controlling the meniscus, removes ribbing. It is therefore of interest to study the behavior of the flow within this range of string positions.

Using the free-surface visualization technique, the shape of the meniscus in contact with the string is measured for several $[Ca_1, Ca_2]$ combinations at constant $G = 0.0163$ with $S$ ranging between 1/3 and 3.0. However, only results with $S = 1$ will be discussed in detail in this article, with general hints for $S \neq 1$. For each $[Ca_1, Ca_2]$ pair, at least nine different positions of the string are investigated to study the resulting flow field. Figure 5 shows the resulting profile after processing of the digital image displayed in Figure 2 ($Ca_1 = Ca_2 = 2{,}0$). The string appears as a dashed line. Its position is estimated from a least-square fit between its visible experimental profile and a circle with the same diameter. This procedure has to be followed because of an observed sag of the string with respect to the holding arms, which can be attributed to viscous drag (Decré, 1994). In this experiment, the tension of the string is not controlled, so the sag cannot be controlled either; the actual position of the string has therefore to be measured, as reported in Figure 6. In Figure 5, the meniscus is clearly divided in two films, connecting to the string at a contact line. These films undergo a rapid relaxation to achieve a nearly constant thickness, as in the free meniscus case.

As in Decré et al. (1995a), it is possible to measure the thickness $h_i$ along each film, and, following an argument by Moffatt (1977), to calculate the dimensionless partial flow rates $\Omega_i = Q_i/h_o U_i$ from the dimensionless thicknesses $\lambda_i = h_i/h_o$, by taking gravity into account

$$\Omega_i = \lambda_i - \frac{\lambda_i^3}{3}\frac{Bo}{Ca_i} \tag{1}$$

where $Bo = \rho g h_o^2/\sigma$ is the local Bond number.

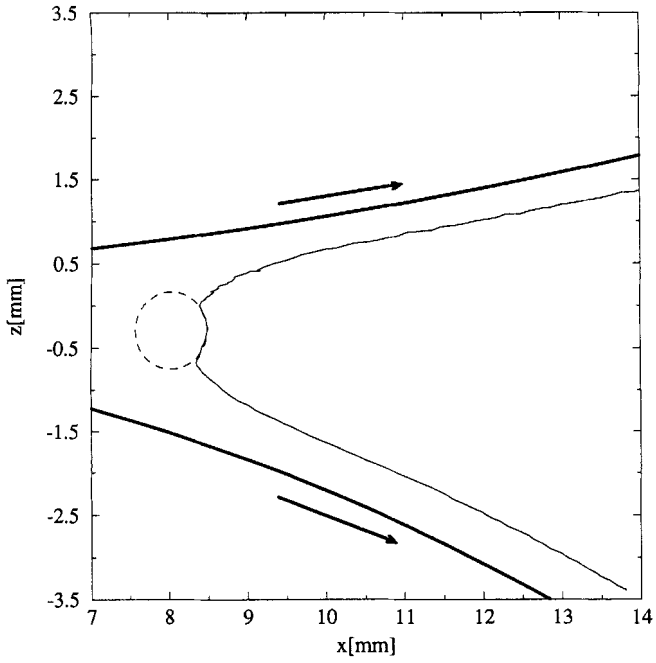


**Figure 5. Interface profile after processing Figure 2.**

The rotation of the cylinders follows the arrows. $Ca_1 = Ca_2 = 2.0$; string position $x_{str} = 8.02$ mm; $z_{str} = -0.29$ mm.

The dimensionless total flow rate is then calculated from its definition

$$\Omega = Q/\left(h_o \frac{U_1 + U_2}{2}\right) = 2(S\Omega_1 + \Omega_2)/(S+1) \qquad (2)$$

$\Omega$ is theoretically equal to 4/3 for fully immersed rolls (Ballal and Rivlin, 1976). The predictions with models taking the interface into account never depart much from this value (Savage, 1982; Coyle et al., 1986). Experimental results are less decisive, as $\Omega$ values up to 1.52 could recently be attributed to indirect feeding effects (Decré et al., 1995a).

A detailed study of the influence of the string position on the advective mass transfer is now presented for $Ca_1 = Ca_2 = 2.0$. The set of actual string positions under investigation is displayed in Figure 6. Each position is numbered to ease interpretation of subsequent results.

The values of the dimensionless total flow rate $\Omega$ as a function of the streamwise position of the string $x_{str}$ are presented in Figure 7. The precision on $\Omega$-estimates is 0.05; it is displayed as errors bars. Each value of $\Omega$ is averaged over all transverse positions at each mean value of $x_{str}$ (filled symbols). The points taken into account in the $\Omega$-average are displayed as corresponding empty symbols. Starting from a constant value of 1.57 at $x_{str} = 8.8$ mm, the total flow rate then decreases when the string goes deeper toward the gap ($x_{str} \leq 8.0$ mm) getting closer to the standard 4/3 value for the free meniscus, but never reaching it. Note from Figure 7 that most of the measurement points for different transversal positions of the string displayed as a series of identical empty symbols fall within the error bars around their average value. This shows that the total flow rate depends only marginally on $z_{str}$. It is clear that the presence of the string significantly perturbs the flow, though no rigorous demonstration is available to explain this flow rate excess. A tentative explanation is to assume that the string, by simultaneously suppressing the free surface boundary condition for pressure and accelerating the flow due to the restriction of the channel width, imposes a lower downstream pressure boundary condition than in the free meniscus case. From the lubricating flow analysis proposed by Savage (1984), it is possible to estimate the pressure difference ($\Delta p$) required across the fluid bead to produce the observed flow rate increase: $\Delta p \approx 2.10^3$ Pa would yield $\Omega \approx 1.55$ under the present experimental conditions. Strictly speaking, the lubrication theory does not hold anymore in the vicinity of the string because of rapid changes in the channel width, so the preceding argument is conjectured to provide some order of magnitude for $\Delta p$ before sounder analyses become available. Simulations of the flow by means of the spectral element fluid analysis program Nekton, Version 2.85, support the preceding analysis (Nekton is a registered trademark of Nektronics Inc. and the MIT, and is supported by Fluent Inc.). The results of Figure 7 give strong evidence of the fact that the streamwise position of the string affects the total flow rate, with limited influence of its transverse position.

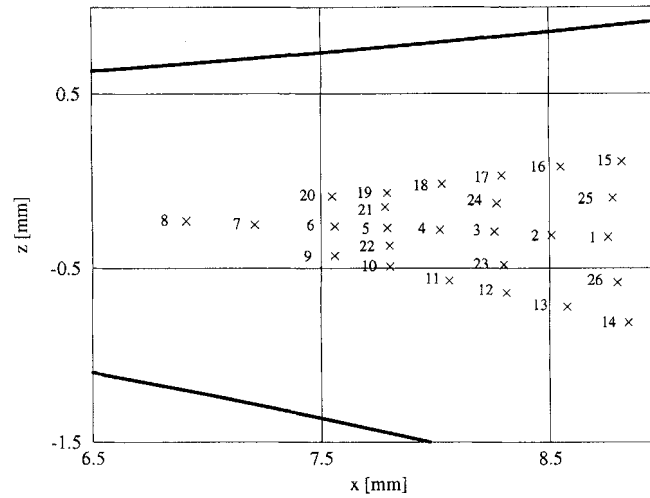


**Figure 6. Actual string positions.**

$Ca_1 = Ca_2 = 2.0$.

A major result concerns the control of the partial flow rates applied on each cylinder. By symmetry, if gravity and the roll radii asymmetry are neglected—typical assumptions in lubrication theory models (Savage, 1982), the validity of which is discussed elsewhere (Decŕe et al., 1995a)—, the dimensionless partial flow rates $\Omega_i$ must be equal when $S = 1$ (Savage, 1982; Coyle et al., 1986). Figure 8 presents the dependence of those partial flow rates as a function of the relative string-cylinders distance $d_1/d_2$, where $d_i$ is the distance separating the surface of the string and the cylinder $i$

$$d_i = \sqrt{(x_{str} - x_i)^2 + (z_{str} - z_i)^2} - R_i - \phi/2 \qquad (3)$$

Figure 8 clearly demonstrates the control that the transverse position of the string exerts on the distribution of the partial flow rates. Whereas the free meniscus case would ideally provide $\Omega_1 = \Omega_2$, here the string obviously monitors the films via contact lines. As a consequence, the flow rate is

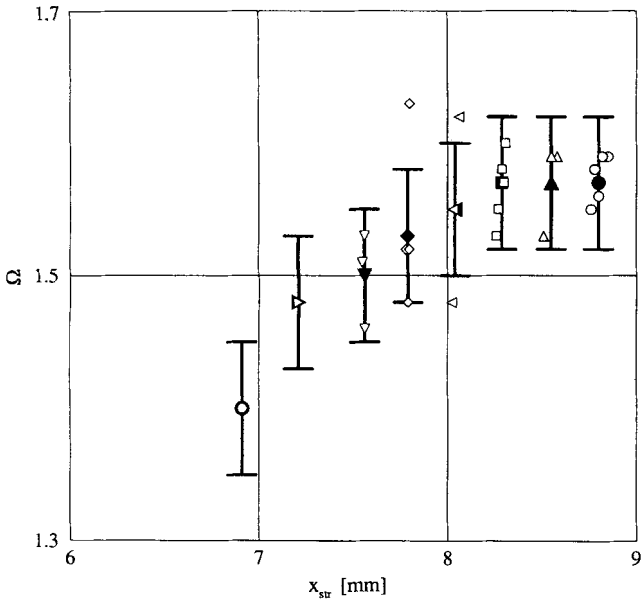


**Figure 7. Dimensionless total flow rate $\Omega$ as a function of the streamwise position of the string $x_{str}$.**

Empty symbols correspond to measured points; filled symbols show the average of the corresponding empty symbols; the error bars reflect the 0.05 accuracy on the measurement of $\Omega$. $Ca_1 = Ca_2 = 2.0$.

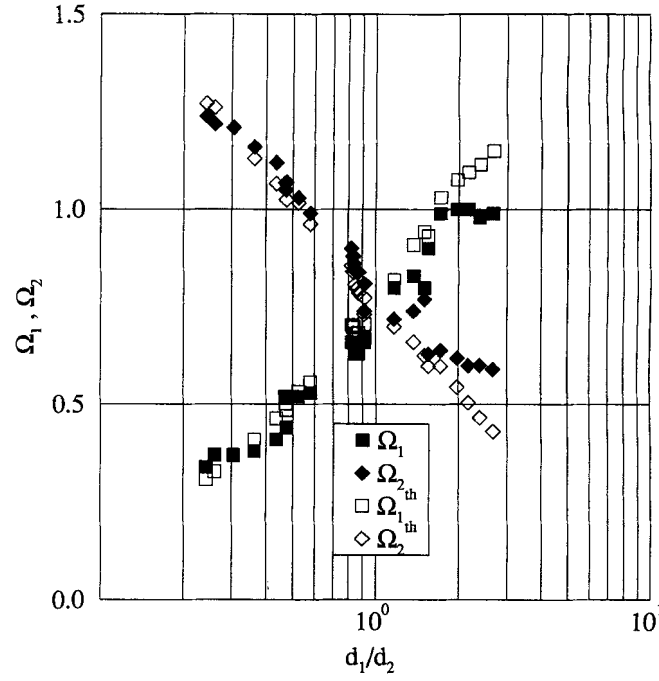


**Figure 8. Dimensionless partial flow rates $\Omega_i$ as a function of the relative string-cylinders distance $d_1/d_2$.**

Filled symbols correspond to measured points; empty symbols are the corresponding theoretical values based on the hypothesis $\Omega_1/\Omega_2 = d_1/d_2$. $Ca_1 = Ca_2 = 2.0$ ($S = 1$). Note the semi-log scale.

smaller on the cylinder to which the string is closer. In Figure 8, $\Omega_1 > (<)\ \Omega_2$ when $d_1 > (<)\ d_2$. It should be noted that all string positions performed according to the scheme given in Figure 6 are displayed in Figure 8; therefore, the results possess much different $x_{str}$ coordinates. The existence of smooth $\Omega_i = f(d_1/d_2)$ curves shows clearly that the partial flow rates are pretty much independent of the streamwise coordinate of the string.

Figure 8 also provides a test for the following hypothesis: if one assumes that $\Omega_1/\Omega_2 = d_1/d_2$, then with $S = 1$ in Eq. 2, one gets

$$\Omega_1^{th} = \Omega \frac{d_1/d_2}{(1 + d_1/d_2)}$$

$$\Omega_2^{th} = \Omega \frac{1}{(1 + d_1/d_2)} \qquad (4)$$

The result of Eq. 4 is displayed in Figure 8 with empty symbols. In applying Eq. 4, $\Omega$ has been computed from Eq. 2 using experimental values. One sees in Figure 8 that for values of $d_1/d_2$ up to 2., Eq. 4 describes very well the flow rate distribution. Some saturation appears at higher values of $d_1/d_2$, as if $\Omega_2$ could not decrease below 0.59. No explanation is currently available for this behavior.

An important quantity from a practical point of view is the relative variation of each partial flow rate for maximum transverse string displacement: $\Delta\Omega_i/\Omega_i = 2(\Omega_i^{max} - \Omega_i^{min})/(\Omega_i^{max} + \Omega_i^{min})$, where $\Omega_i^{max}$ and $\Omega_i^{min}$ are respectively the maximum and minimum partial flow rates over the range of transverse positions. The quantity $\Delta\Omega_i/\Omega_i$ provides a measure of the extent to which it is possible to vary a given partial flow rate without having to modify the speed ratio, as would be the case in standard roll coating (Savage, 1982). In Figure 8, one obtains $\Delta\Omega_1/\Omega_1 \approx 0.95$ and $\Delta\Omega_2/\Omega_2 \approx 0.75$. The asymmetry could be attributed to gravity effects or roll asymmetry. The same figures are obtained for $Ca_m = 1.0$ and 4.0 at $S = 1$. To achieve the same order of relative variation in a free meniscus case would require the speed ratio to vary in the range [0.15, 2.6]. Such values are prohibited in practice, due to increased mechanical hazards when rolls with such speed differences spin close to one another. String control thus presents a major advantage as to the flexibility of coating thickness selection.

Another interesting feature appears when the cylinders are rotating at different speeds ($S \neq 1$): $\Delta\Omega_1/\Omega_1$ reaches values as high as 1.7 ($S = 0.33$). While the total flow rate still depends only marginally on $z_{str}$, the relative variation of partial flow rate is enhanced on the slower roll. This follows from total flow rate conservation. Thickness selection flexibility can consequently be increased by selecting $S \neq 1$.

### *Apparent contact lines*

In order to understand how the string controls both the total flow rate and its distribution in partial flow rates, as well as the elimination of ribbing, details of the flow have to be investigated, in particular the apparent contact conditions on the string. In the present study, the classical, macroscopic approach to contact lines is followed; for a state-of-the-art discussion of those problems, refer to de Gennes (1985) and Dussan V. (1987). The apparent contact conditions are defined in Figure 9: to each film corresponds an apparent contact line, defined by its angular position $\alpha_i$ with respect to the string, and its apparent contact angle $\gamma_i$ formed between

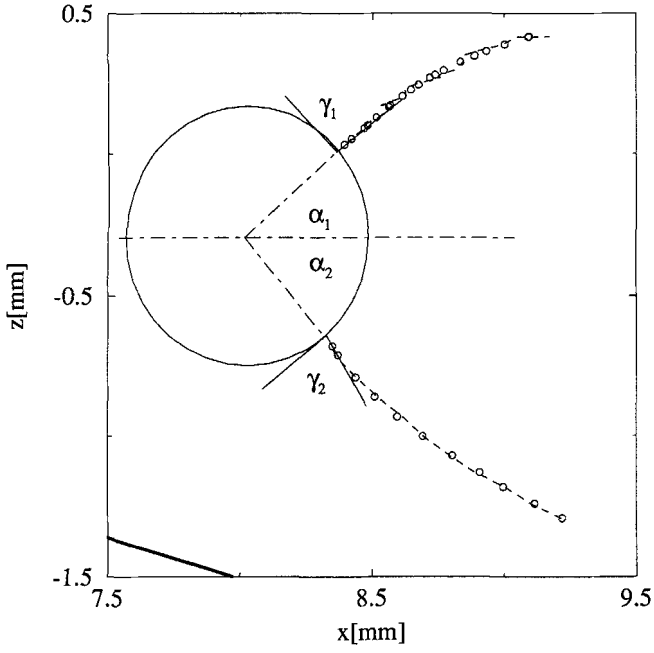


**Figure 9. Principle of the determination of the position $\alpha_i$ of each apparent contact line, and of the apparent contact angle $\gamma_i$.**

$x_{str} = 8{,}02$, $z_{str} = -0{,}29$.

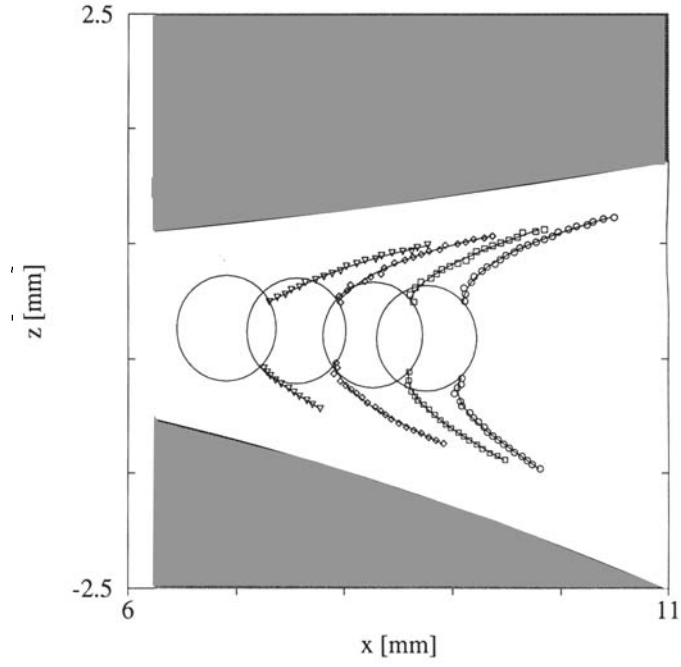


**Figure 10. Evolution of string-film contact conditions as $x_{str}$ decreases.**

Successive string positions correspond to points 1, 3, 6, 8, on Figure 6; the string is equidistant from the rolls.

the tangent to the contacting film and the solid surface. From experimental profiles such as those presented in Figure 5, providing a resolution of 15 $\mu$m, it is possible to estimate the apparent contact conditions with an accuracy of $\pm 5°$ on $\alpha_i$ and $\pm 10°$ on $\gamma_i$.

Figure 10 illustrates the evolution of contact conditions with the depth of the string for constant working conditions at $Ca_1 = Ca_2 = 2.0$. As the string goes deeper toward the gap, the contact lines "crawl" leaving a smaller portion of unwetted string ($\alpha_i$ decrease approximately from 50° to 35°). Simultaneously, the apparent contact angles increase (approximately from 30° to 90°). Some observations have to be pointed out here. First, the large variation of static contact angles contradicts the fact that $\gamma_i$ needs to be well-defined (or at least within the receding and advancing contact angle values in case of contact-angle hysteresis (Dussan V., 1987)). Secondly, the working fluid, silicone oil (dimethylpolysiloxane with linear chain) is well-known for its strong wetting properties: it achieves perfect wetting (zero contact angle) on all but purposefully prepared surfaces. To the best of our knowledge, even the ethoxyled coating of the nylon string should not prevent total wetting. Experimental interface profiles such as shown in Figure 9 would require the interface to bend dramatically within less than 0.05 mm to cope with the latter perfect wetting condition. Lastly, obtaining experimental information about contact angle selection is still needed to better understand, and calculate many coating problems where a contact line is present. This is illustrated in a recent study of the so-called "teapot" effect by Kistler and Scriven (1994), with a Galerkin/finite-element analysis. As in the present study, the teapot effect (flows analogous to that of tea from the spout of a teapot) is qualitatively influenced by contact properties. In such cases, a flowing liquid forms a static contact line with the underlying solid. Kistler and Scriven (1994) have studied this problem by using constant "quasi-static" contact angle values and comparing the position of the computed contact line with experiments. Their work led to the conclusion that the paradigm of quasi-static contact angle is valid, although no direct experimental estimation of the contact angle was made. On the contrary, the present study provides some evidence—though difficult so far to clarify from a theoretical point of view—that the contact angle varies with the flow conditions. This issue of particular importance for future computational solutions of akin problems.

## Conclusions

In this article, a microscopic method to visualize the interface is applied to the quantitative study of the influence of a string brought into contact with the meniscus of an asymmetric roll coating problem. The efficiency of this technique to remove the ribbing instability is clearly demonstrated. The partial and total flow rates are measured as a function of the string position, from the knowledge of the complete profile of the interface. The measured total flow rate is generally larger than in the corresponding free meniscus case, but decreases when the string is moved closer to the gap. On the other hand, the transverse position of the string controls the distribution of partial flow rates on each cylinder, following fairly well the distribution hypothesis $\Omega_1/\Omega_2 = d_1/d_2$. These results are of particular potential interest to industrial applications, as they confirm a simple way to eliminate ribbing and set coating film thicknesses independently of the speed ratio.

Work is still necessary before tackling technological aspects to further investigate fundamental aspects of the proc-

ess: the mechanism by which the string controls the flow is not yet clarified; in particular, several open questions remain about film-string contact conditions; the wetting phenomena which come into play will have to be elucidated, as they constitute an important issue in the computational future of such problems.

## Acknowledgments

The authors wish to thank A.-M. Cazabat, M. Rabaud, M. D. Savage, and P. J. Wicks for stimulating discussions, as well as E. Jabé and J. Missart for their technical assistance. Use of Eq. 4 was suggested by M. Rabaud. M. Decré was supported by a von Karman Institute doctoral fellowship.

## Notation

$A$ = amplitude of ribbing
$Ca_m$ = mean capillary number ( = $\mu U_m/\sigma$ )
$\bar{h}$ = average thickness of the ribbed film
$Q$ = flow rate
$S$ = speed ratio ( = $U_1/U_2$ )
$U$ = tangential speed of cylinder
$x$ = streamwise coordinate
$z$ = transverse coordinate

### *Greek letters*

$\alpha$ = angular position of the contact line
$\gamma$ = apparent contact angle
$\lambda$ = dimensionless film thickness

### *Superscripts*

min = minimum
max = maximum
th = theoretical

## Literature Cited

Adachi, K., T. Tamura, and R. Nakamura, "Coating Flows in a Nip Region and Various Critical Phenomena," *AIChE J.*, **34**(3), 456 (1988).

Ballal, B. Y., and R. S. Rivlin, "Flow of a Newtonian Fluid between Eccentric Rotating Cylinders: Inertial Effects," *Arch. Rat. Mech. Anal.*, **62**, 237 (1976).

Benkreira, H., M. F. Edwards, and W. L. Wilkinson, "Ribbing Instability in the Roll Coating of Newtonian Fluids," *Plast. Rubb. Process. and Appl.*, **2**(2), 137 (1982).

Carter, G. C., and M. D. Savage, "Ribbing in a Variable Speed Two-Roll Coater," *Math. Eng. Ind.*, **1**(1), 83 (1987).

Coyle, D. J., C. W. Macosko, and L. E. Scriven, "Stability of Symmetric Film-Splitting between Counter-Rotating Cylinders," *J. Fluid Mech.*, **216**, 437 (1990).

Coyle, D. J., C. W. Macosko and L. E. Scriven, "Film Splitting Flows in Forward Roll Coating," *J. Fluid Mech.*, **171**, 183 (1986).

Decré, M., "Etude Expérimentale des Comportements de l'Interface dans l'Enduisage par Rouleaux," Doctoral Thesis, Univ. Paris VI, France (1994).

Decré, M., and J. M. Buchlin, "An Extra Thin Laser Sheet Technique Used to Investigate Meniscus Shapes by Laser Induced Fluorescence," *Exp. Fluids*, **16**(5), 339 (1994).

Decré, M., E. Gailly, and J.-M. Buchlin, "Meniscus Shape Experiments in Forward Roll Coating," *Phys. Fluids* **7**(3), 458 (1995a).

Decré, M., E. Gailly, J. M. Buchlin, and M. Rabaud, "Spatio-Temporal Intermittency in a Roll Coating Experiment," *Spatio-Temporal Patterns* (SFI Studies in the Sciences of Complexity), P. E. Cladis and P. Palffy-Muhoray, eds., Addison-Wesley, p. 561 (1995b).

de Gennes, P. G., "Wetting: Statics and Dynamics," *Rev. Mod. Phys.*, **57**(3), 827 (1985).

Dussan V., E. B., "On the Spreading of Liquids on Solid Surfaces: Static and Dynamic Contact Lines," *Ann. Rev. Fluid Mech.*, **11**, 371 (1987).

Hasegawa, T., and K. Sorimachi, "Wavelength and Depth of Ribbing in Roll Coating and its Elimination," *AIChE J.*, **39**(6), 935 (1993).

Kistler, S. F., and L. E. Scriven, "The Teapot Effect: Sheet-Forming Flows with Deflection, Wetting and Hysteresis," *J. Fluid Mech.*, **263**, 19 (1994).

Michalland, S., M. Rabaud, and Y. Couder, "Transition to Chaos by Spatiotemporal Intermittency in Directional Viscous Fingering," *Europhys. Lett.*, **22**(1), 17 (1993).

Moffatt, H. K., "Behaviour of a Viscous Film on the Outer Surface of a Rotating Cylinder," *J. Mécanique*, **16**(5), 651 (1977).

Rabaud, M., S. Michalland, and Y. Couder, "Dynamical Regimes of Directional Viscous Fingering: Spatiotemporal Chaos and Wave Propagation," *Phys. Rev. Lett.*, **64**(2), 184 (1990).

Savage, M. D., "Mathematical Model for the Onset of Ribbing," *AIChE J.*, **30**(6), 999 (1984).

Savage, M. D., "Mathematical Models for Coating Processes," *J. Fluid Mech.*, **117**, 443 (1982).

*Manuscript received Nov. 1, 1994 and revision received Sept. 19, 1995.*